

CuInSe₂-Based Near-Infrared Photodetector

Sung-Tae Kim ¹, Ji-Seon Yoo ¹, Min-Woo Lee ¹, Ji-Won Jung ¹ and Jae-Hyung Jang ^{2,*}

¹ School of Electrical Engineering and Computer Science, Gwangju Institute of Science and Technology (GIST), Cheomdangwagi-ro, Buk-gu, Gwangju 61006, Korea; sungtaekim@gist.ac.kr (S.-T.K.); jiseon0208@gist.ac.kr (J.-S.Y.); minu0001@gm.gist.ac.kr (M.-W.L.); jeongjw11@gm.gist.ac.kr (J.-W.J.)

² School of Energy Engineering, Korea Institute of Energy Technology, Ujeong-ro, Naju-si 58217, Korea

* Correspondence: jjang@kentech.ac.kr

Abstract: Near-infrared (NIR) photodetectors have interesting roles in optical fiber communications and biomedical applications. Conventional NIR photodetectors have been realized using InGaAs and Ge, of which the cut-off wavelengths exceed 1500 nm. Si-based photodetectors exhibit limited external quantum efficiency at wavelengths longer than 1000 nm. By synthesizing a CuInSe₂ compound on a glass substrate, photodetectors that can detect optical wavelengths longer than 1100 nm have been realized in this study. The bandgap energies of the CuInSe₂ thin films were tuned by varying the Cu/In ratio from 1.02 to 0.87. The longest cut-off wavelength (1309 nm) was obtained from a CuInSe₂ thin film having a Cu/In ratio of 0.87. The responsivity of the photodiode was measured under the illumination of a 1064 nm laser light. The photo responses exhibited linear response up to 2.33 mW optical illumination and a responsivity of 0.60 A/W at −0.4 V.

Keywords: CuInSe₂; photodetector; near infrared; bandgap energy; cut-off wavelength



Citation: Kim, S.-T.; Yoo, J.-S.; Lee, M.-W.; Jung, J.-W.; Jang, J.-H. CuInSe₂-Based Near-Infrared Photodetector. *Appl. Sci.* **2022**, *12*, 92. <https://doi.org/10.3390/app12010092>

Academic Editors: Eun-Chel Cho and Hongsun Jee

Received: 5 December 2021

Accepted: 22 December 2021

Published: 22 December 2021

Publisher's Note: MDPI stays neutral with regard to jurisdictional claims in published maps and institutional affiliations.



Copyright: © 2021 by the authors. Licensee MDPI, Basel, Switzerland. This article is an open access article distributed under the terms and conditions of the Creative Commons Attribution (CC BY) license (<https://creativecommons.org/licenses/by/4.0/>).

1. Introduction

Nowadays, near-infrared (NIR) photodetectors which can convert optical signals to electrical signals are getting considerable interest for night-vision imaging, optical fiber communications, biomedical imaging, vegetation monitoring, and security applications due to the strong propagation and low attenuation characteristics of NIR light [1–6]. Conventionally, InGaAs and Ge-based photodetectors with cut-off wavelengths exceeding 1500 nm have been used for NIR photodetectors. Si-based photodetectors are challenging when used to detect the NIR wavelength range and show low external quantum efficiency due to their low cut-off wavelength of 1100 nm [7,8]. However, Ge-based photodetectors suffer from a high dark current (~10 mA/cm²) that is orders of magnitude higher than the ~0.5 μA/cm² of InGaAs photodetectors. This leads to low signal-to-noise ratio (S/N) and responsivity [9–11]. InGaAs-based photodetectors have issues related to expensive manufacturing processes [12,13]. Recently, Cu(In, Ga)Se₂ (CIGS) thin films have become considered one of the most prominent candidates for NIR photoactive layers [14–16].

Polycrystalline copper-indium-gallium-selenide (CIGS) thin films exhibit very promising properties such as competitive stability, a high absorption coefficient of ~10⁵ cm^{−1} (two orders of magnitude higher than that of Si), and an adjustable direct energy bandgap (1.04–1.67 eV) [17,18]. CIGS has gained a reputation as a highly efficient thin film solar cell. The CIGS solar cells have reached a power conversion efficiency (PCE) of 23.35% at laboratory scale [19]. The performance improvement in CIGS solar cells has proven the potential utilization of CIGS thin films for NIR photodetectors. The CIGS thin films can be deposited on top of various substrates such as glass, polyimide, stainless steel, and silicon (Si) so that a CIGS thin film can be utilized to realize NIR photodetectors on various material platforms. Because little research has been reported regarding CIGS as photodetectors, more effort is needed to meet the requirement of the cut-off wavelength needed for operating in the NIR region [20–22].

In the work reported in this paper, copper-indium-selenide (CuInSe_2 , CISE) thin films were investigated as NIR photoactive layers. To achieve high PCE with CIGS, Ga content is added to the CISE thin film to form Ga grading. As the Ga content increases, the bandgap of CIGS increases and shows tunable bandgap characteristics [23,24]. The CIGS thin film optimized for photovoltaic applications contains 8.5% of Ga. When this amount of Ga is incorporated into a CIGS thin film, its cut-off wavelength is limited to 1059.9 nm. To extend the photo-detection capability to the longer wavelength, CISE thin film without Ga is interesting. Therefore, we aimed to fabricate CISE thin film with a bandgap near 0.95 eV. A structure of Al/Ni/aluminum-doped ZnO/i-ZnO/CdS/CISE/Mo was grown on a soda-lime-glass (SLG) substrate to realize a CISE-based photodetector able to detect optical wavelengths longer than 1100 nm. The bandgap energies of the CISE thin films were tuned by varying the Cu/In ratio. The device performance of these CISE-based photodetectors was investigated via the morphological and optical properties of the CISE thin films.

2. Materials and Methods

2.1. Fabrication of CISE Thin Film Photodetectors

CISE thin film photodetectors were fabricated on top of an SLG substrate. The SLG substrates were cleaned to remove organic contamination using acetic acid and deionized water prior to depositing the back contact layer. Molybdenum with a thickness of 1.0 μm was sputtered on SLG as a back contact layer with sputtering power of 300 W under low Ar pressure of 2 mTorr. The CISE layer was deposited using a three-stage co-evaporation process, which is shown in Figure 1a. The In_2Se_3 precursor layer was deposited during the first stage with a substrate temperature of 350 $^\circ\text{C}$, followed by Cu and Se evaporation during the second stage with a substrate temperature of 550 $^\circ\text{C}$. In the third stage, In and Se were co-deposited. Then the films were cooled within a flux of Se until the substrate temperature dropped to 350 $^\circ\text{C}$. The 60 nm-thick CdS layer was subsequently deposited using a chemical bath deposition method. After RF magnetron sputtering of a transparent conducted oxide (TCO) layer consisting of a 70 nm thick i-ZnO layer and a 350 nm thick aluminum-doped ZnO layer (ZnO), a metal electrode consisting of a 50 nm thick Ni adhesion layer and 1 μm thick aluminum was deposited by e-beam evaporation to complete fabrication of the CISE based photodetectors. The 65 nm thick magnesium fluoride (MgF_2) thin film was used for the antireflection coating to minimize the surface reflection. Schematic designs of the CISE thin film photodetectors are shown in Figure 1b. The diameter of the exposed area of the CISE-based photodetectors was 2 mm.

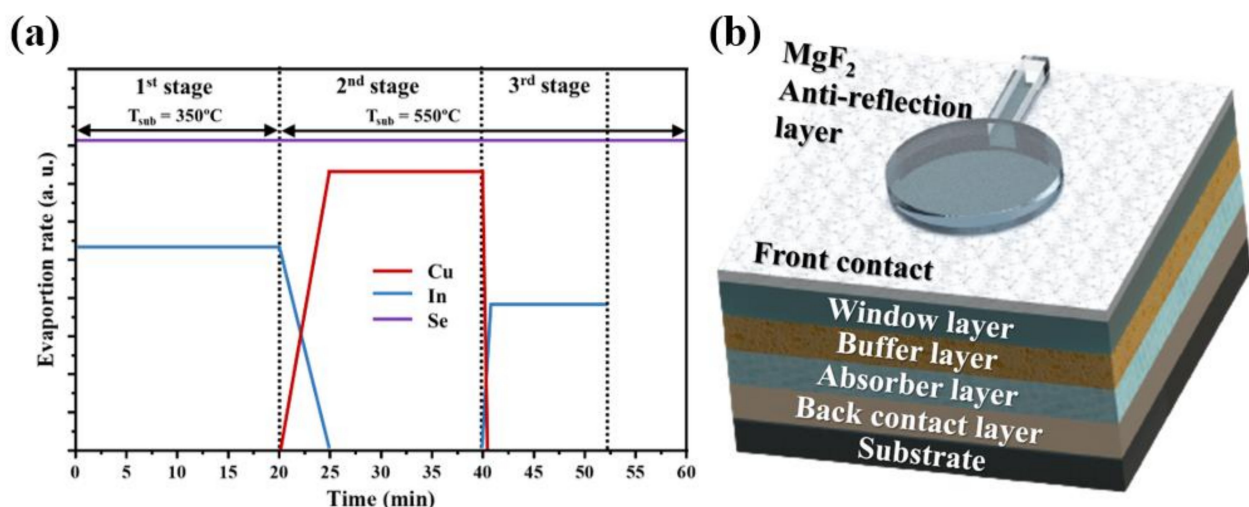


Figure 1. (a) Schematic of the three-stage co-evaporation process. (b) Schematic designing of CISE-based photodetectors.

2.2. Measurement Details

The surface morphology of the synthesized CISE layers was characterized by scanning electron microscopy (SEM, S-4700, Hitachi, Tokyo, Japan). For crystallographic analysis, X-ray diffraction patterns were recorded using an X-ray diffractometer (XRD, X'Pert PRO, Malvern Panalytical, Malvern, UK) with a Cu target (1.5406 Å) and a 1.4 kW power X-ray generator. The Raman Spectra of CISE layers were obtained using a Raman spectroscopy system (LabRam HR800, Horiba Jobin-Yvon, Bensheim, Germany) equipped with a 512 nm and 325 nm excitation laser operated at room temperature. The topographical study was performed using atomic force microscopy (AFM, XE-100, Park Systems, Suwon, South Korea) in non-contact mode with a PPP-NCHR tip (Si). Its force constant and scanning rates were 42 N/m and 0.3 Hz, respectively. The overall Cu/In composition ratio of the CuInSe thin films were confirmed by X-ray fluorescence measurements (XRF, X-Strata980, Malvern Panalytical, Malvern, UK). The refractive index and extinction coefficient of the CISE layer was measured using an Ellipsometer (Elli-SE, Ellipso Technology, Suwon, South Korea). External quantum efficiency (EQE) was measured using an incident photon-to-electron conversion efficiency measurement system (QEX7 series, PV Measurements Inc., Boulder, CO, USA) under a 75 W xenon lamp light source (UXL-75XE, Ushio, Tokyo, Japan). The wavelength of the laser diode used for optical illumination was 1064 nm. The incident optical power was measured using an optical power sensor (1930F-IG, Newport, Irvine, CA, USA). The nominal spot size of the illuminated light that passed through the fiber was <9 μm. Dark current and photocurrent were measured using a semiconductor parameter analyzer (HP 4155A, Agilent, Santa Clara, CA, USA).

3. Results and Discussion

3.1. CuInSe₂ Thin Film with Low Bandgap

A CIGS-based photodetector with a wider spectral range extending into the NIR region could be a candidate for an NIR photodetector. For higher sensitivity in the NIR region, a high-quality photodetector operating in the NIR region using low-bandgap CISE thin film must be realized. The bandgap of CIGS (1.04–1.67 eV) is still too high for use in the NIR region. To achieve a bandgap of about 0.95 eV with a cut-off wavelength of 1305 nm, CISE thin films were grown by the full three-stage process with different durations for the second stage. CISE thin films with Cu/In composition ratios of 1.27 to 0.87 were fabricated.

Figure 2 shows top-view SEM images of CISE thin films grown on the Mo/SLG. The surfaces of CISE films with Cu/In ratios of 0.87 to 0.95 exhibit sharp polyhedral-shaped morphology. The well-faceted polyhedral-shaped grains imply that CISE thin film has a chalcopyrite phase. The grain sizes of CISE films increase as the Cu content increases. For the Cu/In ratios of 0.87 and 0.95, the approximate grain sizes were determined to be about 0.59 and 1.26 μm, respectively. In the Cu-rich state, where the Cu/In ratios are 1.27 and 1.11, the grains exhibited particle-like shapes, and their sizes were 0.91 and 1.14 μm, respectively. The particle-like shapes are ascribed to a large amount of Cu-Se compounds.

Figure 3a shows the Raman spectra for the CISE layers. The CISE layers with Cu/In ratios of 1.27 and 1.11 exhibit the A1 mode of the Cu-Se compound, which means an excess amount of Cu. As the Cu/In ratio decreased, the E mode of CISE increased. The highest intensity of A1 mode of CISE (with a Cu/In ratio of 1.27) could be due to the effect of the Cu-Se compound. The XRD patterns in Figure 3b indicate that all of the CISE films have a chalcopyrite crystal structure with a preferred orientation of (112). Even the XRD patterns of all samples did not show an apparent intensity difference. The CISE thin film with Cu/In ratio of 0.95 was expected to have the highest crystallinity from the Raman spectra results.

The refractive index (n) and extinction coefficient (k) values were measured using an ellipsometer. The measured n and k values are shown in Figure 4a. The refractive index and extinction coefficient of CISE layers increased as the Cu/In ratio decreased, which suggests that the bandgap of CISE thin film decreased as the Cu/In ratio decreased. The wavelength-dependent absorption coefficients of the CISE layers were extracted from the

extinction coefficients. As shown in Figure 4b, the absorption coefficient increased with the decreasing Cu/In ratio.

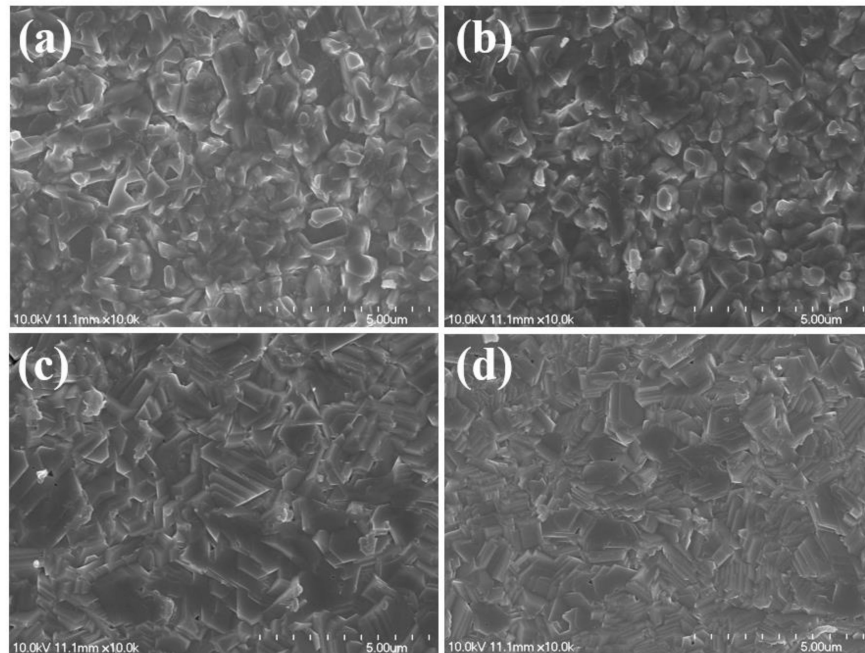


Figure 2. SEM images of CISe thin films with Cu/In ratios of (a) 1.27, (b) 1.11, (c) 0.95, and (d) 0.87.

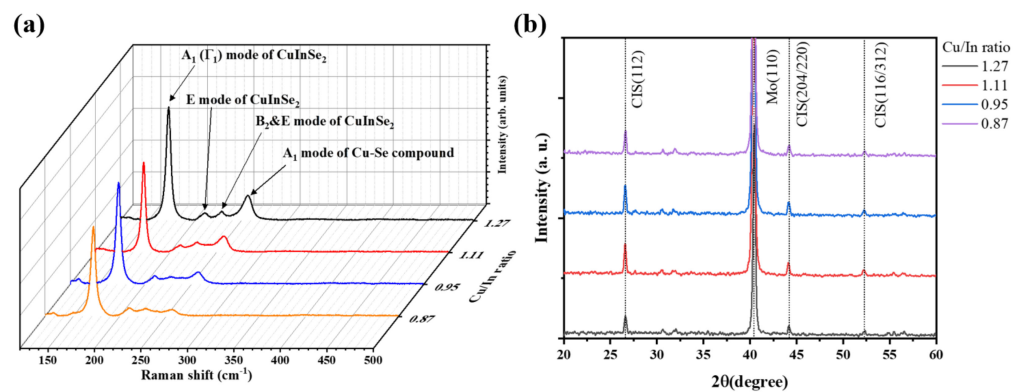


Figure 3. (a) Raman spectra and (b) XRD patterns of the CISe thin films with different Cu/In ratios.

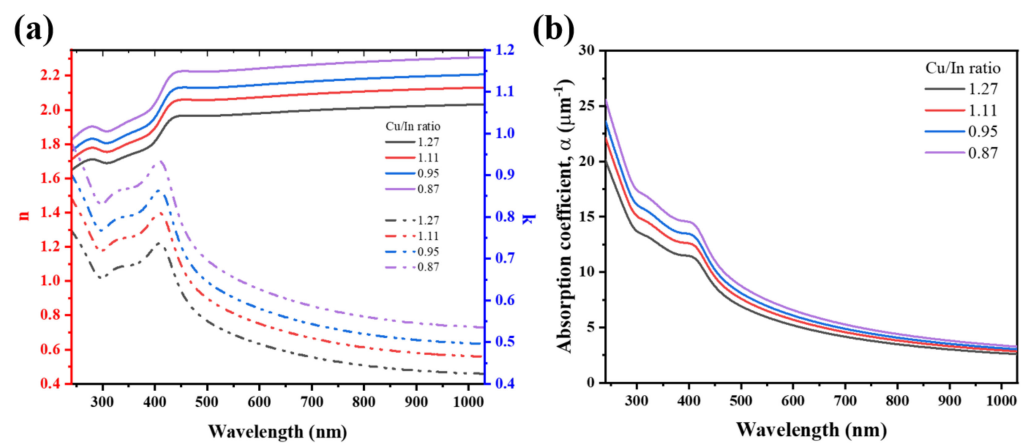


Figure 4. (a) Refractive index, n , extinction coefficient, k , (b) the absorption coefficients of the CISe layers with variable Cu/In ratios.

3.2. CuInSe₂-Based Photodetectors

CISE layers with Cu/In ratios of 0.87, 0.93, 0.94, and 1.02 were utilized to fabricate the photodetectors. The Cu-rich CISE layers, with Cu/In ratios of 1.27 and 1.11, exhibited a Cu-Se compound-related high-defect density on their surfaces, which implies that they are unsuitable for device applications.

The external quantum efficiency (EQE) curves of the CISE thin-film photodetectors with various Cu/In ratios are compared in Figure 5a. The cut-off wavelengths were extracted by extrapolating the EQE curves as shown in the inset of Figure 5a and were utilized to calculate bandgap energies. The bandgap energies of the CISE thin films were tuned by varying the Cu/In ratio from 0.87 to 1.02. As the Cu/In ratio decreased, the bandgap energy decreased, which indicates that an increased cut-off wavelength was realized. The longest cut-off wavelength (1309 nm) was obtained from the CISE thin film having the Cu/In ratio of 0.87. Figure 5b shows the bias current–voltage (I–V) characteristics of the CISE thin-film photodetector in the dark and under 1064 nm laser illumination whose power ranged from 0.83 to 2.33 mW. The CISE-based photodetector with the Cu/In ratio of 0.93 exhibited the dark current density of 28.82 mA/cm² and the differential resistance of 13.24 kΩ at −0.4 V. The low differential resistance is due to the large shunt leakage current. The dark current and responsivity values of the CISE-based photodetector were compared with those of the previously reported CIGS-based photodetectors in Table 1. Further material growth optimization is required to reduce the dark current and to enhance the differential resistance of the CISE-based photodetectors. In the forward biased condition, the current was almost constant, exhibiting the photovoltaic mode of the device. In the reverse biased condition, the current increased gradually with increasing laser power densities up to 2.33 mW, exhibiting a linear response. This current linear response dependency on the incident optical power is favorable for the photodetectors. The responsivity of the CISE thin-film photodetector was 0.52 and 0.60 A/W at 0 V and −0.4 V, respectively.

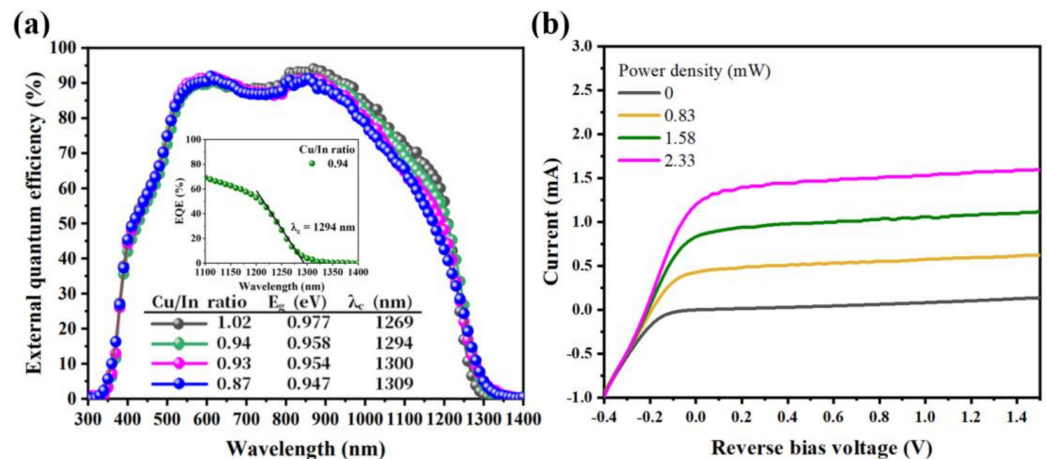


Figure 5. (a) External quantum efficiency (EQE) curves of the CISE photodetectors measured at the bias voltage of −0.4 V. The inset figure shows the method to estimate the cut-off wavelength (λ_c) from the EQE curve. (b) Current–voltage characteristics of the photodetectors with the Cu/In ratio of 0.93 measured under 1064 nm wavelength.

Table 1. Comparison of dark current values of CIGS and CISE-based photodetectors reported in previous literature.

Device Structure	Dark Current	Responsivity (A/W)	References
Solution-processed CIGS	0.3 mA/cm ² @ −0.4 V	0.34 @ 980 nm, 1mW/cm ²	[14]
ZnO/CdS/Al ₂ O ₃ /CIGS	22.2 nA/cm ² @ 0 V	0.54 @ 880 nm	[15]
Ga ₂ O ₃ /CIGS	1 nA/cm ² @ 0 V	—	[25]
CISE	28.82 mA/cm ² @ −0.4 V	0.6 @ 1064 nm	This work

4. Conclusions

Low bandgap CISE thin-film photodetectors for operating in NIR were demonstrated. Low bandgap CISE thin films were grown to improve the photo-absorption properties in the NIR using a three-stage co-evaporation process. The bandgap energies of the CISE thin films were tuned by varying the Cu/In ratio from 1.02 to 0.87. When the bandgap wavelengths of CISE thin films were extracted from the external quantum efficiency of the photodetectors, the wavelengths increased as the Cu/In ratio decreased. The longest cut-off wavelength of 1300 nm was obtained from the CISE thin film having the Cu/In ratio of 0.87. The responsivity of the photodiode was measured under the illumination of a 1064 nm laser light. The photocurrent of the photodetector showed linear dependence on an optical power intensity up to 2.33 mW optical illumination and responsivity of 0.60 A/W under -0.4 V. This work shows that a CISE-based photodetector could be a prominent candidate for a photodetector operating in NIR.

Author Contributions: S.-T.K.: conceptualization, formal analysis, investigation, writing of original draft. J.-S.Y.: methodology, M.-W.L.: investigation, J.-W.J.: methodology, investigation. J.-H.J.: writing, review, and editing. All authors have read and agreed to the published version of the manuscript.

Funding: This work was carried out at GIST with support by the Korea Institute of Energy Technology Evaluation and Planning (KETEP) and the Ministry of Trade, Industry and Energy (MOTIE) of the Republic of Korea (No. 20183010014310). It was also supported by a GIST Research Institute (GRI) grant funded by GIST in 2021, and a National Research Foundation of Korea (NRF) grant funded by the Korean government (Ministry of Science, ICT, and Future Planning) (No. 2017R1A2B3004049).

Conflicts of Interest: The authors declare no conflict of interest.

References

1. Lee, W.Y.; Ha, S.; Lee, H.; Bae, J.H.; Jang, B.; Kwon, H.J.; Yun, Y.; Lee, S.; Jang, J. High-Detectivity Flexible Near-Infrared Photodetector Based on Chalcogenide Ag_2Se Nanoparticles. *Adv. Opt. Mater.* **2019**, *7*, 190812. [[CrossRef](#)]
2. Sargent, E.H. Infrared quantum dots. *Adv. Mater.* **2005**, *17*, 515–522. [[CrossRef](#)]
3. Liu, Z.; Tao, L.; Zhang, Y.; Zhou, G.; Zhu, H.; Fang, Y.; Wu, G.; Yang, D.; Chen, H. Narrowband Near-Infrared Photodetector Enabled by Dual Functional Internal-Filter-Induced Selective Charge Collection. *Adv. Opt. Mater.* **2021**, *9*, 2100288. [[CrossRef](#)]
4. Surdo, S.; Carpignano, F.; Merlo, S.; Barillaro, G. Near-Infrared Silicon Photonic Crystals with High-Order Photonic Bandgaps for High-Sensitivity Chemical Analysis of Water-Ethanol Mixtures. *ACS Sens.* **2018**, *3*, 2223–2231. [[CrossRef](#)]
5. Miao, J.; Zhang, F. Recent progress on highly sensitive perovskite photodetectors. *J. Mater. Chem. C* **2019**, *7*, 1741–1791. [[CrossRef](#)]
6. Sargent, E.H. Solar cells, photodetectors, and optical sources from infrared colloidal quantum dots. *Adv. Mater.* **2008**, *20*, 3958–3964. [[CrossRef](#)]
7. Liu, C.; Guo, J.; Yu, L.; Li, J.; Zhang, M.; Li, H.; Shi, Y.; Dai, D. Silicon/2D-material photodetectors: From near-infrared to mid-infrared. *Light Sci. Appl.* **2021**, *10*, 123. [[CrossRef](#)] [[PubMed](#)]
8. Huang, Z.; Carey, J.E.; Liu, M.; Guo, X.; Mazur, E.; Campbell, J.C. Microstructured silicon photodetector. *Appl. Phys. Lett.* **2006**, *89*, 14–17. [[CrossRef](#)]
9. Son, B.; Lin, Y.; Lee, K.H.; Chen, Q.; Tan, C.S. Dark current analysis of germanium-on-insulator vertical p-i-n photodetectors with varying threading dislocation density. *J. Appl. Phys.* **2020**, *127*, 203105. [[CrossRef](#)]
10. Gonzalez, M.B.; Simoen, E.; Eneman, G.; De Jaeger, B.; Wang, G.; Loo, R.; Claeys, C. Defect assessment and leakage control in Ge junctions. *Microelectron. Eng.* **2014**, *125*, 33–37. [[CrossRef](#)]
11. Son, B.; Lin, Y.; Lee, K.H.; Wang, Y.; Wu, S.; Tan, C.S. High speed and ultra-low dark current Ge vertical p-i-n photodetectors on an oxygen-annealed Ge-on-insulator platform with GeO_x surface passivation. *Opt. Express* **2020**, *28*, 23978. [[CrossRef](#)]
12. Lapiere, R.R.; Robson, M.; Azizur-Rahman, K.M.; Kuyanov, P. A review of III-V nanowire infrared photodetectors and sensors. *J. Phys. D Appl. Phys.* **2017**, *50*, 123001. [[CrossRef](#)]
13. Verdun, M.; Beaudoin, G.; Portier, B.; Bardou, N.; Dupuis, C.; Sagnes, I.; Haïdar, R.; Pardo, F.; Pelouard, J.L. Dark current investigation in thin P-i-N InGaAs photodiodes for nano-resonators. *J. Appl. Phys.* **2016**, *120*, 084501. [[CrossRef](#)]
14. Kim, J.H.; Han, H.; Kim, M.K.; Ahn, J.; Hwang, D.K.; Shin, T.J.; Min, B.K.; Lim, J.A. Solution-processed near-infrared $\text{Cu}(\text{In,Ga})(\text{S,Se})_2$ photodetectors with enhanced chalcopyrite crystallization and bandgap grading structure via potassium incorporation. *Sci. Rep.* **2021**, *11*, 7820. [[CrossRef](#)] [[PubMed](#)]
15. Yuan, Y.; Zhang, L.; Yan, G.; Cen, G.; Liu, Y.; Zeng, L.; Zeng, C.; Zhao, C.; Hong, R.; Mai, W. Significantly Enhanced Detectivity of CIGS Broadband High-Speed Photodetectors by Grain Size Control and ALD- Al_2O_3 Interfacial-Layer Modification. *ACS Appl. Mater. Interfaces* **2019**, *11*, 20157–20166. [[CrossRef](#)]

16. Qiao, S.; Liu, J.; Niu, X.; Liang, B.; Fu, G.; Li, Z.; Wang, S.; Ren, K.; Pan, C. Piezophototronic Effect Enhanced Photoresponse of the Flexible Cu(In,Ga)Se₂ (CIGS) Heterojunction Photodetectors. *Adv. Funct. Mater.* **2018**, *28*, 1707311. [[CrossRef](#)]
17. Chirilă, A.; Buecheler, S.; Pianezzi, F.; Bloesch, P.; Gretener, C.; Uhl, A.R.; Fella, C.; Kranz, L.; Perrenoud, J.; Seyrling, S.; et al. Highly efficient Cu(In,Ga)Se₂ solar cells grown on flexible polymer films. *Nat. Mater.* **2011**, *10*, 857–861. [[CrossRef](#)] [[PubMed](#)]
18. Ramanujam, J.; Singh, U.P. Copper indium gallium selenide based solar cells—A review. *Energy Environ. Sci.* **2017**, *10*, 1306–1319. [[CrossRef](#)]
19. Nakamura, M.; Yamaguchi, K.; Kimoto, Y.; Yasaki, Y.; Kato, T.; Sugimoto, H. Cd-Free Cu(In,Ga)(Se,S)₂ Thin-Film Solar Cell With Record Efficiency of 23.35 %. *IEEE J. Photovolt.* **2019**, *9*, 1863–1867. [[CrossRef](#)]
20. Aldemir, D.A.; Kaleli, M.; Yavru, A.C. Electrical and photoelectric properties of Yb/CIGS thin film Schottky photodiode. *Sens. Actuators A Phys.* **2020**, *311*, 112091. [[CrossRef](#)]
21. Zeng, X.; Lontchi, J.; Zhukova, M.; Fourdrinier, L.; Qadir, I.; Ren, Y.; Niemi, E.; Li, G.; Flandre, D. High-responsivity broadband photodetection of an ultra-thin In₂S₃/CIGS heterojunction on steel. *Opt. Lett.* **2021**, *46*, 2288. [[CrossRef](#)] [[PubMed](#)]
22. Qiao, S.; Feng, K.; Li, Z.; Fu, G.; Wang, S. Ultrahigh, ultrafast and large response size visible-near-infrared optical position sensitive detectors based on CIGS structures. *J. Mater. Chem. C* **2017**, *5*, 4915–4922. [[CrossRef](#)]
23. Gong, J.; Kong, Y.; Li, J.; Wang, K.; Wang, X.; Zhang, Z.; Ding, Z.; Xiao, X. Enhancing photocurrent of Cu(In,Ga)Se₂ solar cells with actively controlled Ga grading in the absorber layer. *Nano Energy* **2019**, *62*, 205–211. [[CrossRef](#)]
24. Colombara, D.; Werner, F.; Schwarz, T.; Cañero Infante, I.; Fleming, Y.; Valle, N.; Spindler, C.; Vacchieri, E.; Rey, G.; Guennou, M.; et al. Sodium enhances indium-gallium interdiffusion in copper indium gallium diselenide photovoltaic absorbers. *Nat. Commun.* **2018**, *9*, 826. [[CrossRef](#)] [[PubMed](#)]
25. Kikuchi, K.; Imura, S.; Miyakawa, K.; Ohtake, H.; Kubota, M.; Ohta, E. Photocurrent multiplication in Ga₂O₃/CuInGaSe₂ heterojunction photosensors. *Sens. Actuators A Phys.* **2015**, *224*, 24–29. [[CrossRef](#)]